Rate-and-state modeling of injection-induced aseismic slip in the Delaware Basin constrains fault-zone pore pressure changes

Noam Z. Dvory[1], Yuyun Yang[2], and Eric M. Dunham[2,3]

[1]Carbon Science Initiative, Energy and Geoscience Institute, The University of Utah, Salt Lake City, Utah, USA.

[2]Institute for Computational Mathematics and Engineering, Stanford University, Stanford, California, USA.

[3]Department of Geophysics, Stanford University, Stanford, California, USA.

Corresponding author: Noam Z. Dvory (nzd@egi.utah.edu)

Key Points:

- Pressure changes from wastewater injection induce aseismic slip in Delaware Basin
- Coupled pore pressure diffusion and rate-state friction model quantifies required pressure change
- Matching observed slip requires a 5 MPa pressure increase beyond the 1-2 MPa required to initiate slip

Abstract

Recent inversions of InSAR ground surface deformation in the Delaware Basin have revealed aseismic slip on conjugate, semi-optimally oriented normal faults. Slip, occurring over 3-5 years, extends approximately 1 km down-dip, over 10 km along strike, and reaches 23 cm. Several disposal wells are located nearby, suggesting that pressure changes from injection might have induced slip. We develop and calibrate 2D and pseudo-3D coupled pore pressure diffusion and rate-state models with velocity-strengthening friction. Pore pressure diffusion is limited to a high-permeability fault damage zone, and the net influx of fluid is adjusted to match the observed slip. A pressure increase of 1-2 MPa is required to initiate slip. Most aseismic slip occurs at approximately constant friction and ~5 MPa additional pressure increase is needed to reach ~20 cm slip. Our work suggests that models of the type developed here can be used to operationally manage injection-induced aseismic slip.

1 Introduction

Pressure rise from carbon sequestration, enhanced geothermal energy development, wastewater injection, and hydraulic fracturing operations may trigger faults to slip. Although there is growing public awareness of induced seismicity that accompanies the pressure rise, fault slip may also occur aseismically if friction is velocity strengthening, as experiments suggest for many reservoir rocks (Kohli & Zoback, 2013; Guglielmi et al., 2015; Cappa et al., 2019). For velocity-strengthening friction, a continued increase of pressure is required to sustain

ongoing aseismic slip, in contrast to velocity-weakening friction, for which appreciable seismic slip, once initiated, occurs without additional pressure changes. Our study examines aseismic slip in the seismically active southernmost part of the Delaware Basin. The Delaware Basin of west Texas and southeastern New Mexico is the westernmost (and largest) part of the Permian Basin. In the last decade, the significant rise of fluid injection volumes associated with oil and gas development was correlated to induced seismicity (Lomax & Savvaidis, 2019; Savvaidis et al., 2020; Skoumal et al., 2020). Water injection appears to be triggering slip on NW-SE trending normal faults striking parallel to the maximum compressive stress, primarily in the Delaware Mountain Group (Dvory & Zoback, 2021a). This region is critically stressed, with a pore pressure rise of 1-2 MPa required to initiate slip on these semi-optimally oriented faults (Dvory & Zoback, 2021a; Hennings et al., 2021). Substantially larger pressure changes are required to produce the observed aseismic slip.

Ground surface deformation was recorded between March 2015 and March 2020, with most deformation occurring in the last three years (Pepin et al., 2021; Staniewicz et al., 2020). Vertical InSAR deformation (Figure 1a) occurs in regions of hydrocarbon development, and in the south is concentrated along lineaments parallel to the maximum horizontal stress, earthquake location trends, and the newly mapped normal faults in the Delaware Mountain Group (Dvory & Zoback, 2021b; Hennings et al., 2021). Pepin et. al. (2021) inverted for slip on three normal faults near the Reeves/Pecos county border (Figure 1b,c), which are close to 12 disposal wells injecting into the Delaware Mountain Group (Figure 1d). A maximum slip of 23 cm occurred on the middle fault. The earthquakes in this area have relatively small magnitude (<M3.8), with slip of no more than a few centimeters, indicating that most of the observed slip is aseismic. Our objective in this study is to quantify the pressure changes and net fluid influx into the fault zone that is required to match the observed slip, using a coupled pore pressure diffusion and rate-state friction model. We also examine how time-dependent changes in injection influence the amount and timing of aseismic slip.

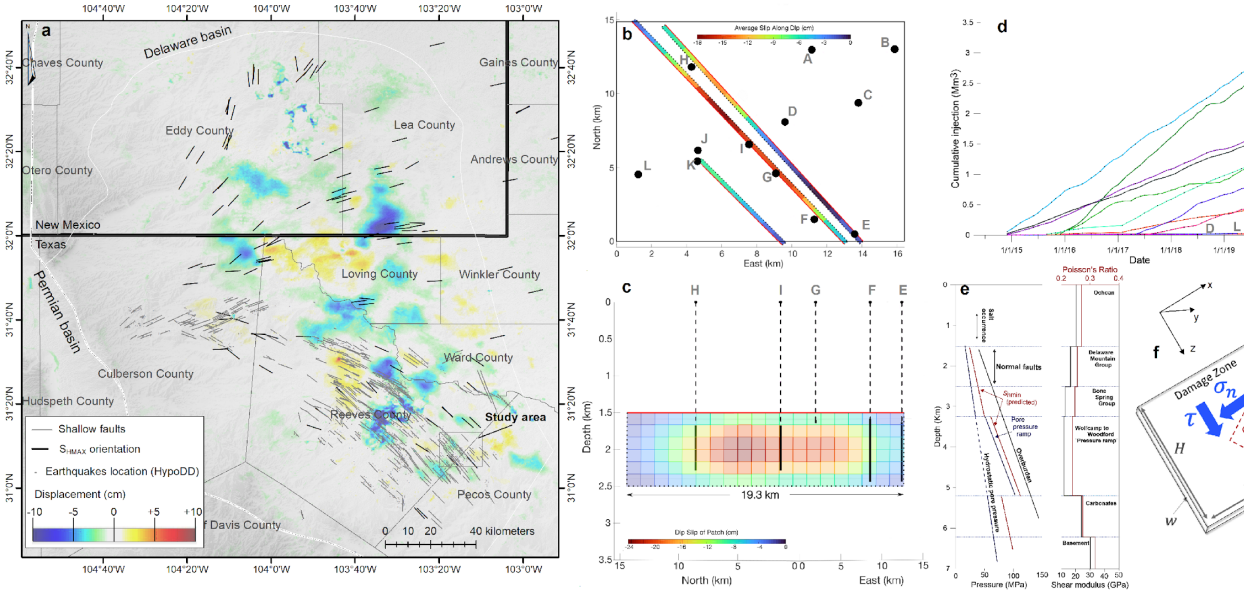

Figure 1. Ground deformation in the Delaware Basin, inferred slip, salt water injection volumes, model parameters and the model schematic. (a) Vertical ground deformation from InSAR analysis of Pepin et al. (2021). Direction of maximum horizontal principal stress is indicated by black lines (Lund Snee & Zoback, 2020). Grey lines indicate normal faults in the Delaware Mountain Group, recently mapped by Hennings et al. (2020). Earthquake epicenters shown by gray dots are from the TexNet relocation catalog. (b) Inferred dip slip from InSAR inversions, shown in map view, over 3 normal faults at the study area (Pepin et al., 2021). Black circles are disposal well locations. (c) Side view of inferred slip. Vertical lines are wells, with uncased intervals shown in solid lines. (d) Cumulative injection in the study area for wells shown in b,c. (e) Stress state and pore pressure in the study area (Dvory and Zoback, 2021a), and the shear modulus and Poisson's ratio calculated from the velocity model of Sheng et al. (2020). (f) Schematic of model, with fluid injection into a permeable fault damage zone, with shear stress and total normal stress $_n$.

2 Stress state, pore pressure, and friction

Integrative geomechanical research indicates that the Delaware Basin is in a normal faulting stress state and that the direction of maximum horizontal compression (S_{Hmax}) in the southern part of the basin is NW-SE (Lund Snee & Zoback, 2018). Dvory and Zoback (2021a) and Hennings et al. (2021) showed that most of the newly mapped shallow normal faults in the Delaware Mountain Group strike sub-parallel to the local direction of S_{Hmax} as Coulomb faulting theory predicts. Dvory and Zoback (2021a) used the Coulomb failure criterion and

assumption that the crust is critically stressed to predict the minimum principal stress (S_{hmin}) and demonstrated, by comparing the results with DFITs and pore pressure measurements, that optimally oriented normal faults (dip = 60^0; fault friction = 0.6) in the Delaware Mountain Group are in frictional failure equilibrium. Figure 1e shows the pore pressure and principal stress gradients near the Reeves/Pecos county border. The pore pressure gradient is essentially hydrostatic in the upper sedimentary section that includes the Delaware Mountain Group and ends at the boundary between the Bone Spring and the Wolfcamp Groups. Below, the pore pressure increases markedly with depth in the upper part of the Wolfcamp and to the Woodford (Rittenhouse et al., 2016). Normal to depleted pore pressure conditions exist in the lower carbonates section. The magnitude of S_{hmin} in Figure 1e is predicted by frictional equilibrium but slightly higher values were also measured in the Wolfcamp shales, presumably due to viscoplastic stress relaxation (Dvory and Zoback, 2021a). The fault of interest in this study is semi-optimally oriented (dip = 70^0) and consequently approximately 1-2 MPa pressure change is required to initiate slip.

To estimate pore pressure rise in the study area, we use the cumulative water disposal volumes from the 12 injection wells shown in Figure 1b. The total injected volume between March 2015 and March 2020 was 14.8 Mm^3. A null hypothesis, which we reject, is that pressurization occurs uniformly over the study region, idealized as a rectangular prism with thickness equal to that of the Delaware Mountain Group (~1 km) and horizontal area shown in Figure 1b (16 km X 15 km), giving a total volume of ~240 km^3. We estimate the pressurization rate as the ratio of total injection rate to storage capacity (the product of volume and specific storage ~10^{-9} Pa^{-1}). The calculated pressurization rate is ~0.01 MPa/year, which is insufficient to initiate slip on the faults of interest over 5 years. Thus we reject the null hypothesis that pressurization occurs uniformly throughout this region. Instead, pressurization must be concentrated in a smaller volume. We continue with the alternative hypothesis that pressurization is predominantly confined to high permeability damage zones surrounding the faults. There is ample evidence for the enhancement of permeability and storage in damage zones which have widths that can reach up to ~100 m (Faulkner & Rutter, 2001; Wibberley, 2002). We are unaware of constraints on the width of damage zones for the faults of interest, so we regard width as an unknown model parameter between 1 and 100 m.

Next we consider constraints on friction. The Delaware Mountain Group is composed of sub-arkosic sandstones and siltstones with some shaley and organic rich layers (Payne, 1976). Friction experiments on similar rocks have been conducted on Berea sandstone (Ikari, 2010), simulated quartz gouge (Marone et al., 1990), arkosic sandstone from the SAFOD hole (Carpenter et al., 2009), and North Sea reservoir sandstones (Samuelson & Spiers, 2012). The experiments show reasonably high friction coefficients f_0 around 0.6 with close to velocity-neutral behavior. We use rate-state friction (Dieterich, 1979; Ruina, 1983; Rice et al., 2001) in which the friction coefficient f depends on slip velocity V and a state variable θ:

$f = f_0 + aln\left(\frac{V}{V_0}\right) + bln\left(\frac{\mathrm{V}}{d_c}\right)$, (1)

$\frac{\mathrm{d}}{\mathrm{dt}} = -\frac{\mathrm{V}}{d_c}\ln\left(\frac{\mathrm{V}}{d_c}\right)$, (2)

where a is the direct effect parameter, b is the state evaluation parameter, V_0 is the reference velocity, V is the slip velocity, d_c is the state evolution distance, is the state variable and t is time. The friction rate parameter a-b is used to quantify velocity-weakening behavior (a-b < 0), which in the absence of other processes altering strength is a requirement for unstable fault slip, and velocity-strengthening behavior (a-b > 0), for which slip is typically aseismic. Based on the experiments above, we select direct effect and state evolution parameters of a = 0.01 and b = 0.009, given our focus on aseismic slip. The characteristic state evolution distance, reference slip velocity, and reference friction coefficient are $\mathrm{d_c}$ = 0.1 mm, $\mathrm{V_0} = 10^{-6}$ m/s, and $\mathrm{f_0}$ = 0.6. The initial state variable is set to $= 4.85\times10^{10}$ s, as appropriate for a long-dormant fault.

3 Coupled pore pressure diffusion and rate-state friction model

We utilize two models in this study. We begin with the 2D model of Zhu et al. (2020) and Yang & Dunham (2021), in which a planar fault is embedded in a linear elastic medium, and the 1D fluid transport and pore pressure diffusion equation is solved simultaneously with the friction and elasticity problem. Our model approximately solves the 2D problem on a vertical cross-section orthogonal to the strike of the fault, resolving pressure diffusion and slip in the down-dip direction while assuming invariance along strike (S1). This is a plane strain problem, whereas our code is for the antiplane shear problem, requiring the use of certain approximations (Supporting Information). We follow this exercise with a pseudo-3D model that captures pressure diffusion and slip variations in the along-strike direction.

The fault is located at y = 0, with y being normal to the fault, and the z axis oriented along the fault in the down-dip direction (Figure 1f). In our 2D modeling, we use a six-layer structural model with piecewise constant elastic properties, taken from Sheng et al. (2020), for the following geological strata: Ochoan, Delaware Mountain Group, Bone Spring Group, Wolfcamp Group to Woodford, the carbonates section and the crystalline basement (Figure 1e, S2). The computational domain extends 20 km down dip and 20 km normal to the fault, and we use grid stretching away from the fault for computational efficiency.

We adopt the quasi-dynamic approximation with radiation damping parameter $_{\mathrm{rad}} = 0.5\mu/\mathrm{c_s}$ (μ, is elastic shear modulus, $\mathrm{c_s}$ is shear wave speed) (Rice, 1993). We integrate the governing equations with an adaptive time-stepping method (Erickson & Dunham, 2014; Allison & Dunham, 2018; Zhu et al., 2020; Yang & Dunham, 2021). Equations 1 and 2 are used to compute the friction coefficient, which is used in the elasticity problem through the fault boundary condition

$\tau = f(\theta, V)(\sigma_0^{'} - p)$, (3)

where $\tau(z,t)$ is the shear stress, $\sigma_0^{'}(z)$ is the initial effective normal stress, and

$p(z,t)$ is the change in pore pressure. Quasi-static elastic stress changes are determined from slip, which is obtained by integrating the slip velocity in time. The initial shear and effective normal stresses are set based on Figure 1e.

Together with the elasticity and friction problem, we solve the 1D linear pore pressure diffusion equation along the fault zone, which is assumed to have uniform width w. A fluid source is introduced at one depth, but as we explain later, the model predictions are relatively insensitive to this depth and even to whether the fluid source is localized or distributed. The fluid source should be regarded as representing the cumulative effects of injection across multiple wells, as will be elaborated upon subsequently. The governing equation for pore pressure is

$$\frac{\partial p}{\partial t} = \frac{\partial}{\partial z}\left(\frac{k}{\eta}\frac{\partial p}{\partial z}\right) + q_0(t)\delta\left(z - z_{\text{inj}}\right), \quad (4)$$

where is the porosity, is the combined fluid and elastic pore compressibility, k is the permeability, is the fluid viscosity, $q_0(t)$ is the injection rate, $\delta\left(z - z_{\text{inj}}\right)$ is the Dirac delta function that places the source at z_{inj}. Regarding parameter values, we set porosity = 0.1 which is representative of fault gouges (Segall & Rice, 1995), compressibility = 10^{-8} Pa^{-1} which is the sum of foliated gouge compressibility (Wibberley, 2002) and water compressibility (Mase & Smith, 1987), viscosity = 10^{-3} Pa s, and permeability k = 10^{-13} m^2 which is an intermediate value between site experiments (Guglielmi et al., 2015; Cappa et al., 2018; Bhattacharya & Viesca, 2019; Larochelle et al., 2021) and basement fault zone permeability (Zhang et al., 2013). This gives a hydraulic diffusivity c = k/( ) = 0.1 m^2/s. To eliminate pressure diffusion below and above the fault zone we use significantly low permeability for the shallow and deep model layers (k = 10^{-16} m^2). The injection is into the middle of the Delaware Mountain Group (Layer 2, z_{inj} = 2.25 km).

In most simulations, we use a constant injection rate, adjusted to match the observed slip. In later examples we consider a time-dependent injection rate. Note that q_0, having units of m/s, quantifies the volume rate of fluid injected per unit fault zone width per unit distance along strike (Figure 1e). To relate the linear rate q_0 to a volumetric rate Q_{net} we estimate the cross-sectional area A through which the fluid flows ($Q_{\text{net}} = q_0 A$). We take A to be the product of L, the along-strike extent of aseismic slip (12 km), and w, the damage zone width. In this way, our injection source can be regarded as arising from multiple wells along strike.

4 Results

Figure 2 presents a simulation for the constant injection rate of $q_0 = 9\times10^{-8}$ m/s. We calibrated the model by adjusting q_0 to approximately match the 23 cm maximum slip after 3 years.

Slip begins after a quiescent period of approximately 170 d, consistent with other studies (Dublanchet, 2019; Yang & Dunham, 2021; Larochelle et al., 2021). During this quiescent period, pressure at the injector increases and diffuses to

other parts of the fault, decreasing the effective normal stress. Because slip is negligible, the shear stress remains approximately constant. Because stress is always equal to strength with rate-state friction, the friction coefficient increases by the direct effect. This continues until slip becomes comparable to the state evolution distance, at which point the friction coefficient drops toward its steady state value and significant slip commences. The peak friction value can be loosely regarded as a static friction coefficient. The pressure change at the onset of significant slip is approximately 1-2 MPa, consistent with the Coulomb prediction, despite a more complex response with rate-state friction.

After this period of slip initiation, sliding continues at the relatively constant steady state friction (Figure 2a,b). Ongoing injection continues to pressurize the fault zone, weakening the fault and causing slip. An additional ~5 MPa pressure increase, beyond the 1-2 MPa to initiate slip, is required to produce the observed ~20 cm maximum slip.

Figure 2c shows that except very early in the simulation, the pressure change is effectively uniform over the Delaware Mountain Group and increases linearly in time. This is because the time scale of interest (~1 yr) is much larger than the hydraulic diffusion time across the down-dip extent of the Delaware Mountain Group, H. Using the commonly used diffusion relation between length and time scales in pressure diffusion studies (e.g., Shapiro et al., 1997; Shapiro & Dinske, 2009), we estimate a diffusion time of $H^2/(4\,c) = 11$ d for H = 1.1 km. Thus, pressure equilibrates rapidly over depth. In this limit, we can integrate the pressure diffusion equation (4) over the down-dip extent H, assuming impermeable boundaries at the top and bottom, to obtain

$$\frac{dp}{dt} = \frac{q_0}{H}. \quad (5)$$

In this limit, there is no dependence on permeability and viscosity (provided that their values render the diffusion time sufficiently short). The predicted pressurization rate for our parameters is dp/dt = 2.6 MPa/yr, which matches the simulation results shown in Figure 2c,d. Because the diffusion time is so short, as compared to the time scales of interest, the pressurization rate is only influenced by the net fluid influx into the fault zone within the Delaware Mountain Group. Therefore the model predictions are effectively independent of the depth of the injector and even whether the fluid source is localized or distributed. Furthermore, it allows us to interpret q_0 as the net influx, defined as the difference between rate at which fluid enters the fault zone and the rate at which fluid leaves the fault zone. Thus, while our model does not explicitly account for leak-off from the fault zone into the surrounding formation, that leak-off can be considered when relating q_0 to the volumetric injection rate Q_{net} from the nearby disposal wells.

The damage zone width is unknown in the study area. We convert our inferred q_0 to Q_{net} for w = 1, 10, and 100 m (S3). Our estimated linear injection rate is $q_0 = 9\times10^{-8}$ m/s, corresponding Q_{net} of 34×10^3 to 34×10^6 m^3/yr, depending on w. Comparing these values with the total injection in the study area or from

nearby wells, it appears that only few percent of the injected volume is required induce slip if the damage zone is narrow, whereas almost all of the injected fluid must enter and remain within the fault zone to induce slip for wide damage zones.

Next we explore the model response to variable injection rate, as is common (Figure 1d). We use a hypothetical, piecewise constant injection rate, chosen to produce a pore pressure rise of about 7.5 MPa and total slip of about 25 cm after 3 years (Figure 3a). As in the constant injection rate case, slip initiates after a pressure increase of 1-2 MPa. Pressurization approximately follows the prediction of equation (6), except for transient adjustments at the scale of several tens of days following each rate step. The duration of these transients is controlled by the diffusion time across the fault, during which time the pressure spatially equilibrates. Slip velocity also tracks the injection rate, with slip ceasing and then resuming when injection is stopped and resumed. Our model therefore suggests that aseismic slip can be controlled in a predictable manner through the injection rate. That said, we caution that the simplicity of this response may be unique to the narrow-fault geometry and 2D approximation that permit the pressure response to be described by the approximate model of equation (6). In this limit, pressurization rate is directly proportional to injection rate, so that pressure remains constant when injection is stopped. This relation would become history-dependent on larger faults or when accounting for along-strike pore pressure diffusion. Similar history dependence would also arise when accounting for leak-off from the fault zone, which would act to depressurize the fault zone.

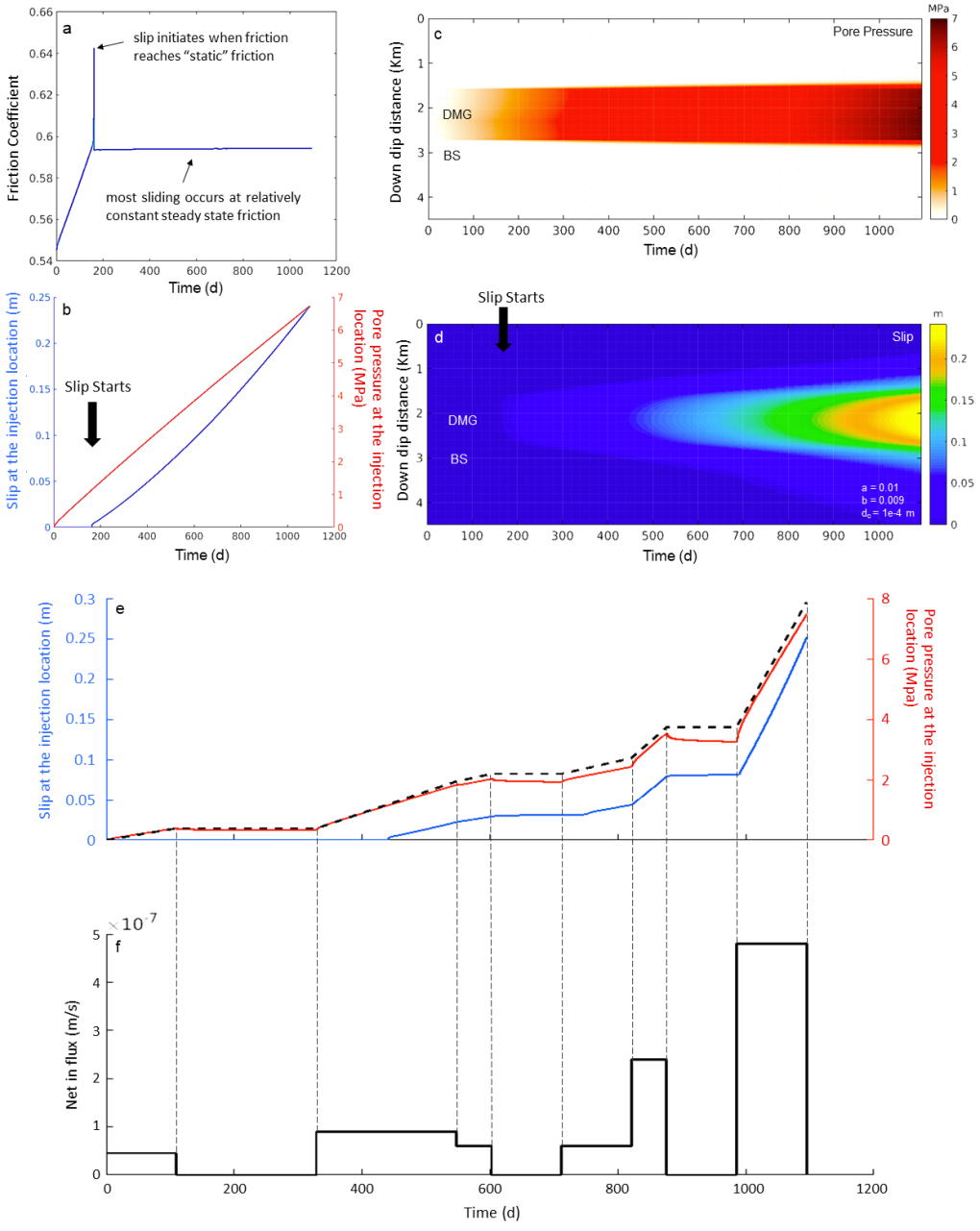

Figure 2. Modeled slip and pore pressure diffusion in response to constant rate ($q_0 = 9\times10^{-8}$ m/s) injection (a)-(e) and a hypothetical time-dependent

injection rate (e)-(f). (a) Friction coefficient evolution at the injection site. (b) Cumulative slip and pore pressure rise at the injection site. (c) Pore pressure rise along the fault. (d) Cumulative slip along the fault. (e) Results for variable injection rate. Red line shows pore pressure change in our simulation. Dashed line shows the prediction of equation (6). Pressure in the simulation is slightly lower than the prediction because it includes leakage from the fault tips. The response might be more complex when accounting for pressure-driven leak-off normal to the fault zone or along-strike pressure diffusion. Cumulative slip is shown by the blue line. (f) Net influx. The aseismic slip stops or resumes with changes in injection rate.

Next we extend our 2D model to a pseudo-3D model in order to account for pore pressure diffusion and multiple injection wells in the along-strike direction. The pseudo-3D model is based on two assumptions, both justified due to the limited down-dip extent of fault slip, H. First, we assume that pressure change is uniform in the down-dip direction, as observed in our 2D simulations. This also implies that the stress drop is spatially uniform in the down-dip direction. Thus pressure and shear stress change depend only on along-strike distance x. Second, we assume that shear stress change at some x is proportional to slip at that x, with proportionality constant from the 2D plane strain crack solution with constant stress drop. For this solution, slip has an elliptical distribution in the down-dip direction, as seen in our 2D simulations. This approximation, which neglects along-strike stress transfer, is the shear version of the well-known tensile fracture elasticity approximation that forms the basis of PKN hydraulic fracture models (Perkins & Kern, 1961; Nordgren, 1972). These assumptions lead to a 1D along-strike pore pressure diffusion equation,

$$\mathrm{wH}\frac{\partial p}{\partial t} = \frac{\partial}{\partial x}\left(\frac{\mathrm{kwH}}{\eta}\frac{\partial p}{\partial x}\right) + \sum Q_i(t)\delta\left(x - x_i\right) \quad (6)$$

where the sum is taken over all wells injecting into the fault zone and $Q_i(t)$ is the volumetric injection rate of well i that is located at along-strike distance x_i. The elasticity response is local at each x, with shear stress given by the spring-slider relation (x,t) = $_0$- s(x,t)- $_{\mathrm{rad}}$V(x,t), where $_0$ is the initial shear stress, s is slip, and the stiffness = μ/(1−)H comes from the 2D plane strain shear crack solution with maximum slip s (e.g., Dieterich, 2007). Elastic properties of the Delware Mountain Group are used to set the stiffness . The initial effective normal stress is 15 MPa and the initial shear stress is 8.175 MPa.

We assume spatially uniform properties, as in our 2D model, and account for three injection wells. These wells, located at x_1 = -8 km, x_2= -1 km, x_3 = 8 km, with x = 0 shown in Figure 1c, have constant injection rates Q_1 = 0.4 Mm^3/yr, Q_2 = 0.2 Mm^3/yr, Q_3 = 0.75 Mm^3/yr that begin at times t = 1.5 yr, 1.5 yr, and 0, respectively, with t = 0 being approximately January 1, 2016. These are somewhat representative of the three injection wells H, I, and F (Figure 1). The model is run for 3 years in most cases. In one case we continue simulating for an additional 2 years, but with no further injection after 3 years, to explore how much additional slip occurs as pressure diffuses away

from the injectors. Without heterogeneity in initial stress, frictional properties, or fluid transport properties, it is impossible to match the spatial distribution of slip, which is biased to the northwest of the injectors, in particular the largest volume well F. We do not believe that sufficient constraints exist to warrant adding heterogeneity to match the inferred slip distribution. Instead, we use the pseudo-3D model to assess the importance of along-strike pressure diffusion in response to multiple injectors.

Using the same fluid transport properties as in the 2D model ($k = 10^{-13}$ m^2, $= 10^{-9}$ Pa^{-1}), the fault damage zone width is selected as $w = 30$ m to produce approximately 30 cm maximum slip. We also consider two additional models, one with $k = 5\times10^{-13}$ m^2 and $w = 15$ m and the second with $k = 5\times10^{-14}$ m^2 and $w = 45$ m, to illustrate how permeability influences the spatial distribution of slip. The damage zone width is adjusted in each case to produce approximately 30 cm maximum slip. In addition, equation (6) shows that Q_i/w, rather than Q_i itself, determines the model response. Consequently, the stated values for Q_i and w can be alternatively interpreted as representing a net injection rate reduced by some constant due to leak-off vertically or normal to the fault zone) with a damage zone that is wider by a factor of 1/ .

The model results, shown in Figure 3, demonstrate that permeability values around $k = 10^{-13}$ m^2 or larger are required to produce slip that is sufficiently spread along-strike away from the injectors. For smaller permeability values, slip is confined to the immediate vicinity of injectors in a manner that is inconsistent with the slip inversions. Significant slip occurs only during active injection, with additional slip after injection occurring primarily in regions away from injectors that experience a pressure increase due to along-strike pressure diffusion away from the injectors. Thus while slip is not quite as synchronized with injection as in our 2D model, our results suggest that aseismic slip can be effectively managed, with minimal time lag, by reducing or stopping injection.

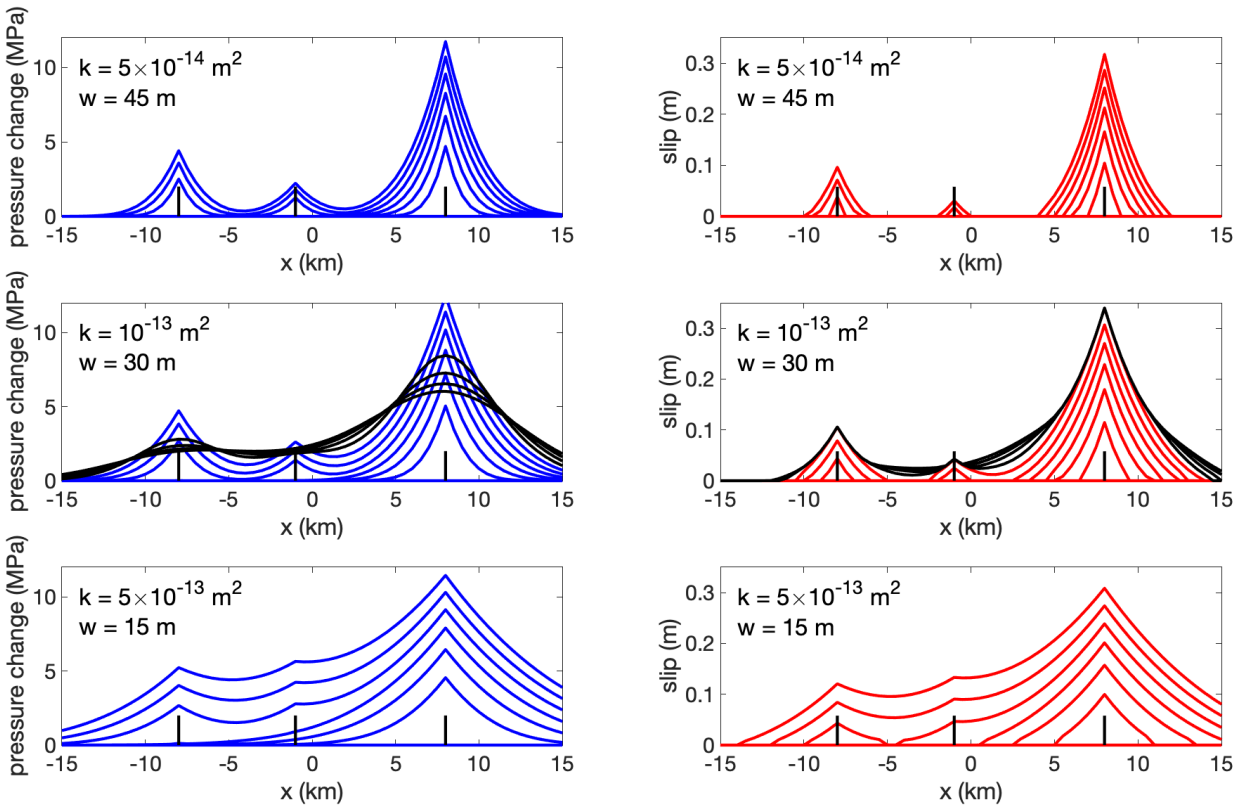

Figure 3: Pseudo-3D model of aseismic slip response to fluid injection at injection locations marked with vertical black lines. Contours of slip and pore pressure change, plotted every 0.5 yr, for various fault damage zone permeabilities and widths: k = 5×10^{-14} m^2 and w = 45 m (top row), k = 10^{-13} m^2 and w = 30 m (middle row), k = 5×10^{-13} m^2 and w = 15 m (bottom row). While all models have approximately the same maximum pressure change and slip, the lower permeability models have more spatially localized response. All simulations are run for 3 years, except the middle row where black curves show an additional 2 year response after injection is ceased; only a small amount of additional slip occurs in this case, primarily in regions away from the injectors.

5 Conclusions

We modeled the aseismic reactivation of shallow normal faults in the southern Delaware basin in response to subsurface wastewater injection, obtaining slip values between 20 and 30 cm that are consistent with slip inversions of InSAR-observed ground deformation. This slip occurred on semi-optimally oriented normal faults in the Delaware Mountain group that trend NW-SE, parallel to the direction of maximum horizontal compression. We present both 2D (vertical cross-section) and pseudo-3D models; the latter exploits the unique fault

geometry in which slip is limited to ~1 km down-dip but extends over 20 km along strike. Our models use initial stresses and pressures that are constrained by measurements and geomechanical analysis, and velocity-strengthening frictional properties from laboratory friction experiments on similar sedimentary rocks and gouges. Fault reactivation in our rate-state friction model requires a 1-2 MPa pressure increase, consistent with Mohr Coulomb analysis. An additional ~5 MPa pressure increase from continued injection is needed to reach the observed ~20 cm slip. We also found that fault slip stops and resumes with minimal time lag when injection is turned on or off, suggesting that aseismic slip can be influenced in a predictable manner by adjusting injection rate. Our results have important implications for mitigating aseismic slip in carbon sequestration, geothermal energy development, and wastewater disposal projects.

Acknowledgments

This work was funded by the Stanford Center for Induced and Triggered Seismicity and the National Science Foundation (EAR-1947448). We thank Karissa Pepin, Mark Zoback, Bill Ellsworth, and Arjun Kohli for helpful conversations.

Data Availability Statement

The source code for the 2D model is available at https://yyang85@bitbucket.org/yyang85/scycle-2.git and the source code for the Pseudo3D model is available at https://github.com/ericmdunham/pseudo3D_I , where a list of input files used for this study is also provided.

References

Allison, K. L., & Dunham, E. M. (2018). Earthquake cycle simulations with rate-state friction and power-law viscoelasticity. *Tectonophysics*, *733*(November 2017), 232–256. https://doi.org/10.1016/j.tecto.2017.10.021

Bhattacharya, P., & Viesca, R. C. (2019). Fluid-induced aseismic fault slip outpaces pore-fluid migration. *Science*, *364*(6439), 464–468. https://doi.org/10.1126/science.aaw7354

Broberg, K. B. (1999). *Cracks and fracture*. Elsevier.

Cappa, F., Guglielmi, Y., Nussbaum, C., & Birkholzer, J. (2018). On the Relationship Between Fault Permeability Increases, Induced Stress Perturbation, and the Growth of Aseismic Slip During Fluid Injection. *Geophysical Research Letters*, *45*(20), 11,012-11,020. https://doi.org/10.1029/2018GL080233

Cappa, F., Scuderi, M. M., Collettini, C., Guglielmi, Y., & Avouac, J. P. (2019). Stabilization of fault slip by fluid injection in the laboratory and in situ. *Science Advances*, *5*(3), 1–9. https://doi.org/10.1126/sciadv.aau4065

Carpenter, B. M., Marone, C., & Saffer, D. M. (2009). Frictional behavior of materials in the 3D SAFOD volume. *Geophysical Research Letters*, *36*(5), 1–5. https://doi.org/10.1029/2008GL036660

Choi, J. H., Edwards, P., Ko, K., & Kim, Y. S. (2016). Definition and classification of fault damage zones: A review and a new methodological approach. *Earth-*

Science Reviews, *152*, 70–87. https://doi.org/10.1016/j.earscirev.2015.11.006

Dieterich, J. H. (2007). *Applications of Rate- and State-Dependent Friction to Models of Fault-Slip and Earthquake Occurrence. Treatise on Geophysics: Second Edition*. https://doi.org/10.1016/B978-0-444-53802-4.00075-0

Dieterich, James H. (1979). Modeling of rock friction 1. Experimental results and constitutive equations. *Journal of Geophysical Research: Solid Earth*, *84*(B5), 2161–2168. https://doi.org/10.1029/JB084iB05p02161

Dublanchet, P. (2019). Fluid driven shear cracks on a strengthening rate-state frictional fault. *Journal of the Mechanics and Physics of Solids*, *132*, 1–20. https://doi.org/10.1016/j.jmps.2019.07.015

Dvory, N. Z., & Zoback, M. D. (2021a). Assessing Fault Slip Potential in a Continuously Varying Stress Field – Application in the Delaware Basin. *American Rock Mechanics Association, 55th US Rock Mechanics/Geomechanics Symposium*.

Dvory, N. Z., & Zoback, M. D. (2021b). Prior Oil and Gas Production Limits the Occurrence of Injection-Induced Seismicity in the Delaware Basin of West Texas and Southeastern New Mexico. *Geology*, *XX*(Xx), 1–6.

Erickson, B. A., & Dunham, E. M. (2014). An efficient numerical method for earthquake cycles in heterogeneous media: Alternating subbasin and surface-rupturing events on faults crossing a sedimentary basin. *Journal of Geophysical Research: Solid Earth*, *119*(4), 3290–3316. https://doi.org/10.1002/2013JB010614

Faulkner, D. R., Mitchell, T. M., Jensen, E., & Cembrano, J. (2011). Scaling of fault damage zones with displacement and the implications for fault growth processes. *Journal of Geophysical Research: Solid Earth*, *116*(5), 1–11. https://doi.org/10.1029/2010JB007788

Faulkner, Daniel R., & Rutter, E. H. (2001). Can the maintenance of overpressured fluids in large strike-slip fault zones explain their apparent weakness? *Geology*, *29*(6), 503–506. https://doi.org/10.1130/0091-7613(2001)029<0503:CTMOOF>2.0.CO;2

Guglielmi, Y., Cappa, F., Avouac, J. P., Henry, P., & Elsworth, D. (2015). Seismicity triggered by fluid injection-induced aseismic slip. *Science*, *348*(6240), 1224–1226. https://doi.org/10.1126/science.aab0476

Hennings, P., Dvory, N. Z., Horne, E., & Zoback, M. D. (2020). Slip Potential and Seismogenic Association of Basement-Rooted Faults in the Delaware Basin, West Texas. *American Geophysical Union, Fall Meeting*.

Hennings, P., Dvory, N., Horne, E., Li, P., Savvaidis, A., & Zoback, M. (2021). Stability of the Fault Systems That Host-Induced Earthquakes in the Delaware Basin of West Texas and Southeast New Mexico. *The Seismic Record*, *1*(2), 96–106. https://doi.org/10.1785/0320210020

Ikari, M. J. (2010). Compositional, Mechanical and hydrological controls on fault slip behavior, (August), 135–187.

Ikari, M. J., Marone, C., & Saffer, D. M. (2011). On the relation between fault strength and frictional stability. *Geology*, *39*(1), 83–86. https://doi.org/10.1130/G31416.1

Kohli, A. H., & Zoback, M. D. (2013). Frictional properties of shale reservoir rocks. *Journal of Geophysical Research: Solid Earth*, *118*(9), 5109–5125. https://doi.org/10.1002/jgrb.50346

Larochelle, S., Lapusta, N., Ampuero, J. P., & Cappa, F. (2021). Constraining Fault Friction and Stability With Fluid-Injection Field Experiments. *Geophysical Research Letters*, *48*(10), 1–11. https://doi.org/10.1029/2020GL091188

Lomax, A., & Savvaidis, A. (2019). Improving Absolute Earthquake Location in West Texas Using Probabilistic, Proxy Ground-Truth Station Corrections. *Journal of Geophysical Research: Solid Earth*. https://doi.org/10.1029/2019JB017727

Lund Snee, J. E., & Zoback, M. D. (2018). State of stress in the Permian Basin, Texas and New Mexico: Implications for induced seismicity. *Leading Edge*, *37*(2), 127–134. https://doi.org/10.1190/tle37020127.1

Lund Snee, J. E., & Zoback, M. D. (2020). Multiscale variations of the crustal stress field throughout North America. *Nature Communications*, *11*(1), 1–9. https://doi.org/10.1038/s41467-020-15841-5

Marone, C., Raleigh, C. B., & Scholz, C. H. (1990). Frictional behavior and constitutive modeling of simulated fault gouge. *Journal of Geophysical Research*, *95*(B5), 7007–7025. https://doi.org/10.1029/JB095iB05p07007

Mase, C. W., & Smith, L. (1987). Effects of frictional heating on the thermal, hydrologic, and mechanical response of a fault. *Journal of Geophysical Research*, *92*(B7), 6249–6272. https://doi.org/10.1029/JB092iB07p06249

Mitchell, T. M., & Faulkner, D. R. (2009). The nature and origin of off-fault damage surrounding strike-slip fault zones with a wide range of displacements: A field study from the Atacama fault system, northern Chile. *Journal of Structural Geology*, *31*(8), 802–816. https://doi.org/10.1016/j.jsg.2009.05.002

Nordgren, R. P. (1972). Propagation of a Vertical Hydraulic Fracture. *Society of Petroleum Engineers Journal*, *12*(04), 306–314. https://doi.org/10.2118/3009-pa

Okada, Y. (1985). Internal deformation due to shear and tensile faults in a half-space. *Bulletin - Seismological Society of America*, *75*(4), 1135–1154. https://doi.org/10.1785/bssa0820021018

Payne, M. W. (1976). Basinal Sandstone Facies, Delaware Basin, West Texas and Southeast New Mexico. *AAPG Bulletin (American Association of Petroleum Geologists)*, *60*(4), 517–527. https://doi.org/10.1306/83d923f2-16c7-11d7-8645000102c1865d

Pepin, K. S., Ellsworth, W. L., Sheng, Y., & Zebker, H. A. (2021). Shallow Aseismic Slip in the Delaware Basin Determined by Sentinel-1 InSAR (in review). *Journal of Geophysical Research - Solid Earth*, 1–43.

Perkins, T. K., & Kern, L. R. (1961). Widths of Hydraulic Fractures. *Journal of Petroleum Technology*, *13*(09), 937–949. https://doi.org/10.2118/89-pa

Rice, J. R. (1993). Spatio-temporal complexity of slip on a fault. *Journal of Geophysical Research*, *98*(B6), 9885–9907. https://doi.org/10.1029/93JB00191

Rice, James R., Lapusta, N., & Ranjith, K. (2001). Rate and state dependent friction and the stability of sliding between elastically deformable solids. *Journal of the Mechanics and Physics of Solids*, *49*(9), 1865–1898. https://doi.org/10.1016/S0022-5096(01)00042-4

Rittenhouse, S., Currie, J., & Blumstein, R. (2016). Using Mud Weights, DST, and DFIT Data to Generate a Regional Pore Pressure Model for the Delaware Basin, New Mexico and Texas. In *Proceedings of the 4th Unconventional Resources Technology Conference*. Tulsa, OK, USA: American Association of Petroleum Geologists. https://doi.org/10.15530/urtec-2016-2450423

Rudnicki, J. W., & Wu, M. (1995). Mechanics of dip-slip faulting in an elastic half-space. *Journal of Geophysical Research*, *100*(B11). https://doi.org/10.1029/95jb02246

Ruina, A. (1983). Slip instability and state variable friction laws. *Journal of Geophysical Research*, *88*(B12), 10359–10370. https://doi.org/10.1029/JB088iB12p10359

Samuelson, J., & Spiers, C. J. (2012). Fault friction and slip stability not affected by Co2 storage: Evidence from short-term laboratory experiments on North Sea reservoir sandstones and caprocks. *International Journal of Greenhouse Gas Control*, *11*(SUPPL), 78–90. https://doi.org/10.1016/j.ijggc.2012.09.018

Savage, H. M., & Brodsky, E. E. (2011). Collateral damage: Evolution with displacement of fracture distribution and secondary fault strands in fault damage zones. *Journal of Geophysical Research: Solid Earth*, *116*(3). https://doi.org/10.1029/2010JB007665

Savvaidis, A., Lomax, A., & Breton, C. (2020). Induced seismicity in the Delaware Basin, west Texas, is caused by hydraulic fracturing and wastewater disposal, 6–9.

Segall, P., & Rice, J. R. (1995). Dilatancy , compaction , and slip instability model hydraulic diffusivity c * (diffusivity / diffusion. *Journal of Geophysical Research*, *100*, 155–171.

Shapiro, S. A., & Dinske, C. (2009). Fluid-induced seismicity: Pressure diffusion and hydraulic fracturing. *Geophysical Prospecting*, *57*(2), 301–310. https://doi.org/10.1111/j.1365-2478.2008.00770.x

Shapiro, S. A., Huenges, E., & Borm, G. (1997). Estimating the crust permeability from fluid-injection-induced seismic emission at the KTB site. *Geophysical Journal International*, *131*(2), 5–8. https://doi.org/10.1111/j.1365-246X.1997.tb01215.x

Sheng, Y., Ellsworth, W. L., & Pepin, K. S. (2020). On the Depth of Earthquakes in the Delaware Basin – A Case Study along the Reeves-Pecos County line. *American Geophysical Union, Fall Meeting*.

Skoumal, R. J., Barbour, A. J., Brudzinski, M. R., Kaven, J. O., & Skoumal, R. J. (2020). Induced seismicity in the Delaware Basin , Texas. https://doi.org/10.1029/2019JB018558

Staniewicz, S., Chen, J., Lee, H., Olson, J., Savvaidis, A., Reedy, R., et al. (2020). InSAR Reveals Complex Surface Deformation Patterns Over an 80,000 km2 Oil-Producing Region in the Permian Basin. *Geophysical Research Letters*, *47*(21). https://doi.org/10.1029/2020GL090151

Wibberley, C. A. J. (2002). Hydraulic diffusivity of fault gouge zones and implications for thermal pressurization during seismic slip. *Earth, Planets and Space*, *54*(11), 1153–1171. https://doi.org/10.1186/BF03353317

Yang, Y., & Dunham, E. M. (2021). Effect of Porosity and Permeability Evolution on Injection-Induced Aseismic Slip. *Journal of Geophysical Research: Solid Earth*, *126*(7), 1–36. https://doi.org/10.1029/2020JB021258

Zhang, Y., Person, M., Rupp, J., Ellett, K., Celia, M. A., Gable, C. W., et al. (2013). Hydrogeologic controls on induced seismicity in crystalline basement rocks due to fluid injection into basal reservoirs. *Groundwater*, *51*(4), 525–538. https://doi.org/10.1111/gwat.12071

Zhu, W., Allison, K. L., Dunham, E. M., & Yang, Y. (2020). Fault valving and pore pressure evolution in simulations of earthquake sequences and aseismic slip. *Nature Communications*, *11*(1), 1–11. https://doi.org/10.1038/s41467-020-18598-z